COBEM 2023 27TH INTERNATIONAL CONGRESS OF MECHANICAL ENGENEERING

ABCM Brazilian Society of Mechanical Sciences and Engineering
27th ABCM International Congress of Mechanical Engineering
December 04-08, 2023, Florianópolis-SC, Brazil

COB-2023-0335
PREDICTION AND CONTROL OF BIFURCATIONS IN ROTOR-FOUNDATION SYSTEMS SUPPORTED BY FLUID-FILM BEARINGS

Arthur Guilherme Mereles
School of Mechanical Engineering, University of Campinas, Mendeleyev Street, 200, 13083-860, Campinas, SP, Brazil
a230355@dac.unicamp.br

Diogo Stuani Alves
Department of Mechanical Engineering, University of Bath, BA2 7AY, Bath, UK.
dsa41@bath.ac.uk

Katia Lucchesi Cavalca
School of Mechanical Engineering, University of Campinas, Mendeleyev Street, 200, 13083-860, Campinas, SP, Brazil
katia@fem.unicamp.br

Abstract. *The use of oil-lubricated bearings is very common in many rotating machines, mainly due to their high load capacity, reliability, and low friction. However, these types of bearings often present instabilities at certain operating speeds. Experimental studies have found two main types of instabilities, namely, oil-whirl and oil-whip. These can be seen as a Hopf bifurcation, which can be either super- or sub-critical, where the former case corresponds to oil-whirl and the latter to oil-whip. Hence, detecting the type of Hopf bifurcation, tells whether one experiences oil-whirl or oil-whip. This work presents an approach to predict Hopf bifurcations by means of the Center Manifold Reduction (CMR) method in rotor-foundation systems. The basis of the approach is to obtain the center manifold of the bifurcating system and study it to learn if the system will present oil-whirl or oil-whip. In addition to predicting the limit cycles that arise in the Hopf bifurcation, it is also proposed a method to control these cycles by means of a nonlinear control force. The idea here is to change the normal form coefficient of the Hopf bifurcation, allowing one to change the instability from oil-whip (more dangerous) to oil-whirl (less dangerous). The control force is applied on the foundation, and thus the approach could be implemented in on-site machines. The method is applied to a simple rotor system modeled by the Finite Element Method (FEM) and supported by a spring-mass-damper foundation. The results of the predicted limit cycles using the CMR, as well as the controlled cycles, are validated by comparing them with the ones obtained via numerical continuation.*

Keywords: *Rotor-foundation system, fluid-film bearings, Hopf bifurcation, center manifold reduction.*

1. INTRODUCTION

Rotating machines, including turbines and generators, commonly incorporate fluid-film bearings due to their reliability and high load capacity. However, the intricate dynamic interaction between the rotating shaft and the fluid medium gives rise to inherent self-excited instabilities in these bearing types. These instabilities result in the transfer of energy from the fluid to the shaft, leading to excessive vibration amplitudes. Through experimental studies, researchers have identified two types of instabilities known as "oil-whirl" and "oil-whip." In the case of oil-whirl, the rotor exhibits a subsynchronous frequency of vibration, approximately $0.5\times$ the shaft's rotational speed. On the other hand, oil-whip involves a non-synchronous frequency that is related to the natural frequency of the rotor (Muszynska, 1988). A notable difference between oil-whirl and oil-whip lies in the behavior of the rotor. In oil-whirl, the rotor reaches a stable limit cycle of oscillation, typically within the bearing clearance. However, in oil-whip, the rotor experiences a significant increase in vibration amplitude, ceasing only upon encountering a physical barrier.

Researchers have attributed the instabilities observed in fluid bearings to a Hopf bifurcation (Wiggins, 2003). This bifurcation leads to the emergence of limit cycles as a parameter, namely the shaft rotational speed, is varied. At the bifurcation point, if the resulting limit cycles are unstable, it corresponds to a *sub-critical* Hopf bifurcation, indicative of oil-whip. On the other hand, a *super-critical* bifurcation corresponds to oil-whirl, where the limit cycles remain stable. Identifying whether oil-whirl or oil-whip occurs relies on determining the type of Hopf bifurcation that arises at the critical speed. Various studies have employed a Taylor expansion of the equations of motion up to the third order for this purpose (Wang and Khonsari, 2006; Miraskari *et al.*, 2017). Although these investigations have focused on simple rotor systems using the Jeffcott model, the approach can be extended to complex turbine-generator systems, as demonstrated

by Chasalevris (2020). Studies on the Hopf bifurcation of rotors indicate that both bearing parameters and shaft flexibility can influence the type of bifurcation observed, thereby determining the occurrence of oil-whirl or oil-whip.

An alternative approach for identifying the type of Hopf bifurcations involves analyzing the system's center manifold. This manifold represents an expansion of the linear center subspace, which corresponds to the mode that becomes unstable at the bifurcation point. By examining the dynamics occurring on the center manifold, it becomes possible to determine the nature of the bifurcation. The advantage of this method is that it allows for inferring the qualitative behavior of the system, even if it is high-dimensional, solely by analyzing the dynamics on the center manifold (Troger and Steindl, 1991). In the study of rotor systems with floating-ring bearings, Boyaci *et al.* (2009) utilized Center Manifold Reduction (CMR). Similarly, Kano *et al.* (2019) employed CMR in combination with static reduction to investigate general rotors with fluid-film bearings. Although the CMR method exhibits good accuracy in detecting the type of bifurcation, it is limited in predicting the size of the limit cycles. This information, however, can be crucial during the design phase of fluid-film bearings.

This work presents a method to determine the limit cycles of oscillation following a Hopf bifurcation in general rotor-foundation systems supported by fluid-film bearings. The key idea behind this approach is to obtain the system's center manifold using the parameterization method for invariant manifolds (Haro *et al.*, 2016; Ponsioen *et al.*, 2020), which offers improved performance compared to the conventional CMR technique. In addition, a method to control the limit cycles that emerge after the bifurcation is proposed, where one is able to change the type of bifurcation and reduce the amplitude of the limit cycles. This control is performed by means of a nonlinear force, which acts solely in the foundation. The idea here is to change the normal form coefficient of the Hopf bifurcation, allowing one to change the instability from oil-whip (more dangerous) to oil-whirl (less dangerous).

2. THEORETICAL BACKGROUND

2.1 Rotor-foundation model

The rotor system studied in this work is depicted in Fig. 1, and it consists of a shaft with diameter d and length L. A disk with diameter D and thickness of h_d is positioned at $x = L/2$ from the left free end, as shown in the figure. The rotor is supported by two identical nonlinear bearings through two journals, which in turn are connected to the supporting structure. The latter is considered a spring-mass-damper system, with mass M_f, and isotropic stiffness and damping coefficients, K_f and C_f. The shaft is modeled using Timoshenko beam elements in the two orthogonal directions; thus, only flexural deformations are considered, while torsion and axial movements are neglected. This is a common approach in the study of rotating machines (Friswell *et al.*, 2010). Also, the disk and journals are considered rigid masses with polar and diametral moments of inertia. The equation of motion of the system can be written in general form as (Cavalca and Okabe, 2011; Mereles *et al.*, 2023),

$$\begin{bmatrix} \mathbf{M_r} & \mathbf{0} \\ \mathbf{0} & \mathbf{M_f} \end{bmatrix} \begin{Bmatrix} \ddot{\bar{\mathbf{x}}}_\mathbf{r} \\ \ddot{\bar{\mathbf{x}}}_\mathbf{f} \end{Bmatrix} + \left(\begin{bmatrix} \mathbf{C_r} + \Omega \mathbf{G_r} & \mathbf{0} \\ \mathbf{0} & \mathbf{C_f} \end{bmatrix} + \mathbf{R}(\Omega) \right) \begin{Bmatrix} \dot{\bar{\mathbf{x}}}_\mathbf{r} \\ \dot{\bar{\mathbf{x}}}_\mathbf{f} \end{Bmatrix} + \left(\begin{bmatrix} \mathbf{K_r} & \mathbf{0} \\ \mathbf{0} & \mathbf{K_f} \end{bmatrix} + \mathbf{S}(\Omega) \right) \begin{Bmatrix} \bar{\mathbf{x}}_\mathbf{r} \\ \bar{\mathbf{x}}_\mathbf{f} \end{Bmatrix} = \mathbf{f_{nl}}(\bar{\mathbf{x}}_\mathbf{r} - \bar{\mathbf{x}}_\mathbf{f}, \dot{\bar{\mathbf{x}}}_\mathbf{r} - \dot{\bar{\mathbf{x}}}_\mathbf{f}) + \mathbf{f_g} + \mathbf{f_c}(\bar{\mathbf{x}}_\mathbf{f}), \quad (1)$$

where $\bar{\mathbf{x}} \in \mathbb{R}^N$ is the nodal displacement vector, N is the total number of DOFs, and the subscripts **r** and **f** denote the rotor and foundation terms, respectively. $\mathbf{M}$, $\mathbf{C}$, $\mathbf{G}$ and $\mathbf{K} \in \mathbb{R}^{N \times N}$ are the mass, damping, gyroscopic and stiffness matrices,

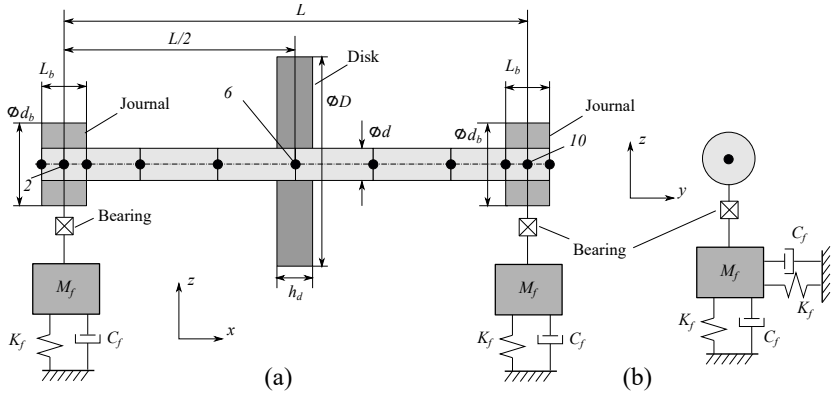

Figure 1: Coordinate system and discretization of the rotor-foundation system: front (a) and side (b) view. (Adapted from Mereles *et al.* (2023)).

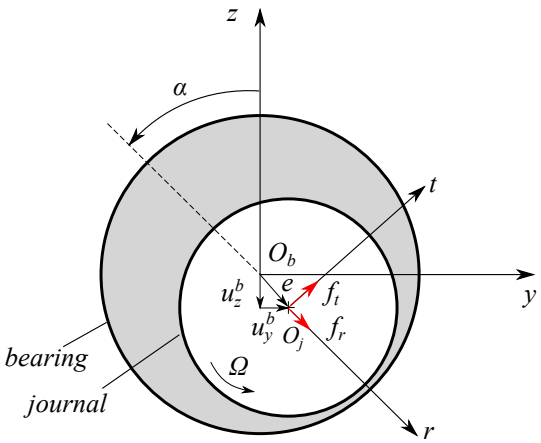

Figure 2: Geometry of the fluid-film bearing

respectively, and Ω is the shaft speed. The effect of the bearings is considered in the matrices $\mathbf{R}$ and $\mathbf{S} \in \mathbb{R}^{N\times N}$, which are the linearized damping and stiffness matrices, and the function $\mathbf{f_{nl}} : \mathbb{R}^{2N} \to \mathbb{R}^N$, are the purely nonlinear components of the bearing forces, that is, what is left after the linearization. Also, the term $\mathbf{f_g} \in \mathbb{R}^N$ denotes the gravity force, which is a constant vector acting at the center of mass of the system and $\mathbf{f_c} : \mathbb{R}^N \to \mathbb{R}^N$ is the control force that is applied at the foundation. The rotor system is considered perfectly balanced, which makes the system autonomous. It is convenient to rewrite Eq. (1) with respect to the equilibrium position by performing a change of variables as,

$$\mathbf{x} = \bar{\mathbf{x}} - \mathbf{x_e}, \tag{2}$$

being $\mathbf{x} = \{\mathbf{x_r} \;\; \mathbf{x_f}\}^T$, $\bar{\mathbf{x}} = \{\bar{\mathbf{x}}_\mathbf{r} \;\; \bar{\mathbf{x}}_\mathbf{f}\}^T$, and $\mathbf{x_e} = \{\mathbf{x_{er}} \;\; \mathbf{x_{ef}}\}^T$ the equilibrium position. The equilibrium position is obtained from Eq. (1) by assuming $\ddot{\bar{\mathbf{x}}}_\mathbf{r} = \ddot{\bar{\mathbf{x}}}_\mathbf{f} = \dot{\bar{\mathbf{x}}}_\mathbf{r} = \dot{\bar{\mathbf{x}}}_\mathbf{f} = 0$. By using Eq. (2), Eq. (1) is rewritten as,

$$\mathbf{M}\ddot{\mathbf{x}} + \mathbf{D}\dot{\mathbf{x}} + \mathbf{K}\mathbf{x} = \mathbf{f_{nl}}(\mathbf{x_r} - \mathbf{x_f} + \mathbf{x_{er}} - \mathbf{x_{ef}}, \dot{\mathbf{x}}_\mathbf{r} - \dot{\mathbf{x}}_\mathbf{f}) + \mathbf{f_g} - \mathbf{K}\mathbf{x_e} + \mathbf{f_c}(\mathbf{x_f} + \mathbf{x_{ef}}) = \mathbf{f}(\mathbf{x}, \dot{\mathbf{x}}), \tag{3}$$

where,

$$\mathbf{M} = \begin{bmatrix} \mathbf{M_r} & \mathbf{0} \\ \mathbf{0} & \mathbf{M_f} \end{bmatrix}, \quad \mathbf{D} = \begin{bmatrix} \mathbf{C_r} + \Omega\mathbf{G_r} & \mathbf{0} \\ \mathbf{0} & \mathbf{C_f} \end{bmatrix} + \mathbf{R}(\Omega), \quad \mathbf{K} = \begin{bmatrix} \mathbf{K_r} & \mathbf{0} \\ \mathbf{0} & \mathbf{K_f} \end{bmatrix} + \mathbf{S}(\Omega). \tag{4}$$

In this work, the bearings that support the rotating shaft are considered to be cylindrical of the fluid-film type. These bearings are widely used in many rotordynamics applications since they can sustain high dynamic loads and display relatively low friction. The forces from the bearings are obtained from the solution of the Reynolds equation, considering the bearing to be infinitely short and using the Gümbel (half-Sommerfeld) boundary condition, and it is given as (Wang and Khonsari, 2006; Miraskari *et al.*, 2017),

$$f_r = -\frac{\mu R L_b^3}{2c_r^2}\left[\frac{2\varepsilon^2(\Omega - 2\dot{\alpha})}{(1-\varepsilon^2)^2} + \frac{\pi(1+2\varepsilon^2)\dot{\varepsilon}}{(1-\varepsilon^2)^{5/2}}\right], \quad f_t = \frac{\mu R L_b^3}{2c_r^2}\left[\frac{\pi(\Omega - 2\dot{\alpha})\varepsilon}{2(1-\varepsilon^2)^{3/2}} + \frac{4\varepsilon\dot{\varepsilon}}{(1-\varepsilon^2)^2}\right], \tag{5}$$

f_r and f_t being the radial and tangential components, measured in the reference frame rotating and whirling with the shaft (See Fig. 2); μ is the fluid viscosity (assumed constant), R the shaft (journal) radius at the bearing, L_b the bearing's length, and c_r the radial clearance. Also, α and $\dot{\alpha}$ denote the angular position of the shaft's center and the whirl speed, while $\varepsilon = e/c_r$ denotes the dimensionless eccentricity. From Fig. 2, one has the following relations,

$$\alpha = \tan^{-1}\left(\frac{u_y^b}{u_z^b}\right), \quad \varepsilon = \frac{1}{c_r}\sqrt{\left(u_y^b\right)^2 + \left(u_z^b\right)^2}, \quad \dot{\alpha} = \frac{u_z^b\dot{u}_y^b - u_y^b\dot{u}_z^b}{c_r^2\varepsilon^2}, \quad \dot{\varepsilon} = \frac{u_y^b\dot{u}_y^b + u_z^b\dot{u}_z^b}{c_r^2\varepsilon}, \tag{6}$$

where $u_y^b = u_{y,\mathbf{r}}^b - u_{y,\mathbf{f}}^b$ and $u_z^b = u_{z,\mathbf{r}}^b - u_{z,\mathbf{f}}^b$ denote the relative horizontal and vertical displacements of the shaft's center at the bearing location. The transformation of the nonlinear force into the fixed reference frame can be done by,

$$f_y = f_r \sin\alpha + f_t \cos\alpha, \quad f_z = f_t \sin\alpha - f_r \cos\alpha. \tag{7}$$

These forces can be implemented in the finite element model by using,

$$\mathbf{f} = \mathbf{f_{by}} f_y + \mathbf{f_{bz}} f_z, \tag{8}$$

$\mathbf{f_{by}}$ and $\mathbf{f_{bz}}$ being Boolean vectors with ones only at the DOFs with bearings and zeros elsewhere. The stiffness $\mathbf{S}$ and damping $\mathbf{R}$ matrices presented in Eq. (1) are obtained from a first-order Taylor expansion of the bearing force given by Eq. (8) (See Mereles *et al.* (2023) on how to implement them in the model).

The higher order terms $\mathbf{f_{nl}}$ consist of cubic and quadratic terms, and they are given as,

$$\mathbf{f_{nl}} = \boldsymbol{\beta}_{(2000)}(u_y^b)^2 + \boldsymbol{\beta}_{(0200)}(u_z^b)^2 + \boldsymbol{\beta}_{(0020)}(\dot{u}_y^b)^2 + \boldsymbol{\beta}_{(0002)}(\dot{u}_z^b)^2 + \boldsymbol{\beta}_{(1100)}\dot{u}_y^b\dot{u}_z^b + \cdots \\ + \boldsymbol{\beta}_{(3000)}(u_y^b)^3 + \boldsymbol{\beta}_{(0300)}(u_z^b)^3 + \boldsymbol{\beta}_{(0030)}(\dot{u}_y^b)^3 + \cdots. \quad (9)$$

In Miraskari *et al.* (2017) one finds closed-form expressions for the higher order coefficients $\boldsymbol{\beta}_{(ijkl)}$. As it will be shown in Section 2.2, the type of bifurcation is mainly defined by the third-order coefficients of the bearing force. Aware of this fact, the control force is assumed as,

$$\mathbf{f_c} = \mathbf{f_{cb}}\gamma(u_{y,\mathbf{f}}^b)^3, \quad (10)$$

$\mathbf{f_{cb}}$ being a Boolean vector, and γ the control force coefficient. The closed-loop control approach adopted is basically a proportional gain controller. In this sense, the control force acts as a cubic spring. Moreover, the control is applied just in the horizontal direction and at the foundation DOFs. This force could be introduced in a real machine through an electromagnetic or hydraulic actuator.

2.2 Center manifold reduction

According to the center manifold theorem, the dynamics of the full system can be studied by what takes place on the center manifold (Troger and Steindl, 1991). This section presents the application of the parameterization method for invariant manifolds (Haro *et al.*, 2016; Ponsioen *et al.*, 2020) to perform a center manifold reduction (CMR). Firstly, the system given by Eq. (3) is rewritten into state-space form, leading to,

$$\dot{\mathbf{w}} = \mathbf{A}\mathbf{w} + \mathbf{g}(\mathbf{w}), \quad (11)$$

where,

$$\mathbf{A} = \begin{bmatrix} \mathbf{0} & \mathbf{I} \\ \mathbf{M}^{-1}\mathbf{K} & \mathbf{M}^{-1}\mathbf{D} \end{bmatrix}, \quad \mathbf{w} = \begin{Bmatrix} \mathbf{x}, & \dot{\mathbf{x}} \end{Bmatrix}^T, \quad \mathbf{g}(\mathbf{w}) = \begin{Bmatrix} \mathbf{0}, & \mathbf{M}^{-1}\mathbf{f}(\mathbf{w}). \end{Bmatrix}^T \quad (12)$$

Next, the state vector $\mathbf{w}$ is expanded in terms of the eigenvectors of the matrix $\mathbf{A} \in \mathbb{R}^{2N\times 2N}$ as,

$$\mathbf{w} = \sum_{i=1}^{2N} \boldsymbol{\phi}^i q_i = [\boldsymbol{\phi}^1 \ \boldsymbol{\phi}^2 \ \cdots \ \boldsymbol{\phi}^{2N}]\mathbf{q} = \boldsymbol{\phi}\mathbf{q}, \quad (13)$$

$\boldsymbol{\phi} \in \mathbb{C}^{2N\times 2N}$ being the matrix with the eigenvectors at its columns, and $\mathbf{q} \in \mathbb{C}^{2N}$ the generalized coordinates. The eigenvectors and adjoint eigenvectors are obtained from the solution of,

$$\mathbf{A}\boldsymbol{\phi}^i = \lambda_i\boldsymbol{\phi}^i, \quad \mathbf{A}^H\boldsymbol{\psi}^i = \lambda_i^*\boldsymbol{\psi}^i, \quad (14)$$

in which $i \in \{1,\cdots,2N\}$, λ_i are the eigenvalues, $\boldsymbol{\psi}^i \in \mathbb{C}^{2N}$ is the ith adjoint eigenvector, * denotes complex conjugation, and H denotes the hermitian (complex conjugate) transpose. The solution of both eigenvalue problems in Eq. (14) is necessary due to the nature of the matrix $\mathbf{A}$, which is in general non-hermitian (Lee, 1993). The eigenvectors and their adjoints can be normalized so as to satisfy,

$$(\boldsymbol{\psi}^j)^H\boldsymbol{\phi}^i = \delta_{ij}, \quad (\boldsymbol{\psi}^j)^H\mathbf{A}\boldsymbol{\phi}^i = \lambda_j\delta_{ij}, \quad (15)$$

δ_{ij} being the Kronecker delta. The conditions above are commonly referred to as biorthonormality conditions (Lee, 1993). By substituting the expansion (13) in Eq. (11), pre-multiplying the equations by $\boldsymbol{\psi}^H$, and using the biorthonormality conditions, one arrives at,

$$\dot{\mathbf{q}} = \boldsymbol{\Lambda}\mathbf{q} + \boldsymbol{\psi}^H\mathbf{g}(\boldsymbol{\phi}\mathbf{q}), \quad (16)$$

where $\boldsymbol{\Lambda} = \mathrm{diag}(\lambda_1,\cdots,\lambda_{2N})$. Equation (16) is the diagonal form of the rotor system given by Eq. (11). Let $\lambda_{1,2}$, with $\lambda_2 = \lambda_1^*$, denote the pair of eigenvalues of the mode that becomes unstable as $\Omega > \omega_w$, ω_w being the instability speed (Note that this might require a reordering of matrices $\boldsymbol{\Lambda}$ and $\boldsymbol{\psi}$, depending on the rotor system). At the instability speed ($\Omega = \omega_w$), the eigenvalues of $\lambda_{1,2}$ become purely imaginary, that is $\mathrm{Re}[\lambda_{1,2}] = 0$, and a Hopf bifurcation occurs. To perform a CMR, one defines the following quantities (Ponsioen *et al.*, 2020),

$$\mathbf{q} = \mathbf{h}(\mathbf{p}), \quad (17a)$$

$$\dot{\mathbf{p}} = \mathbf{r}(\mathbf{p}), \tag{17b}$$

$\mathbf{p} \in \mathbb{C}^2$ being the normal or parameterization coordinates, $\mathbf{h} : \mathbb{C}^2 \to \mathbb{C}^{2N}$ a nonlinear map that relates the original coordinates $\mathbf{q}$ to the normal coordinates $\mathbf{p}$, and $\mathbf{r} : \mathbb{C}^2 \to \mathbb{C}^2$ a function that defines the reduced dynamics for the normal coordinates. This approach is known in the literature as the parameterization method (Haro *et al.*, 2016). By substituting Eq. (17a) into (16), and using Eq. (17b), one arrives at,

$$\frac{\partial \mathbf{h}(\mathbf{p})}{\partial \mathbf{p}}\mathbf{r}(\mathbf{p}) = \mathbf{\Lambda}\mathbf{h}(\mathbf{p}) + \mathbf{g}_1(\mathbf{p}), \tag{18}$$

in which $\mathbf{g}_1 = \boldsymbol{\psi}^H \mathbf{g}\big(\boldsymbol{\phi}\mathbf{h}(\mathbf{p})\big)$. Equation (18) is known as the invariance equation (Haro *et al.*, 2016; Ponsioen *et al.*, 2020), and it consists of a Partial Differential Equation (PDE). The invariance equation is solved expanding $\mathbf{h}$ and $\mathbf{r}$ into multivariate polynomials as,

$$h_i(\mathbf{p}) = H_{i,(1,0)}p_1 + H_{i,(0,1)}p_2 + H_{i,(1,1)}p_1p_2 + \cdots = \sum_{\mathbf{k}} H_{i,\mathbf{k}}\mathbf{p}^{\mathbf{k}}, \tag{19}$$

$$r_j(\mathbf{p}) = R_{j,(1,0)}p_1 + R_{j,(0,1)}p_2 + R_{j,(1,1)}p_1p_2 + \cdots = \sum_{\mathbf{k}} R_{j,\mathbf{k}}\mathbf{p}^{\mathbf{k}}, \tag{20}$$

in which $i \in \{1, \cdots, 2N\}$, $j \in \{1, 2\}$, $\mathbf{k} = (k_1, k_2)$ is a vector with the polynomial indices with $k_i \in \mathbb{N}$, and $\mathbf{p}^{\mathbf{k}} = p_1^{k_1}p_2^{k_2}$. The order of the multivariate polynomial is given by $|\mathbf{k}| = k_1 + k_2$. The coefficients of the polynomials are contained in the multi-dimensional complex arrays $H_{i,\mathbf{k}}$ and $R_{j,\mathbf{k}}$.

By substituting Eqs. (19)-(20) into (18), one has,

$$\sum_{j=1}^{2}\left(\sum_{\mathbf{k}} H_{i,\mathbf{k}}\mathbf{p}^{\mathbf{k}-\mathbf{e}_j}\right)\sum_{\mathbf{k}} R_{j,\mathbf{k}}\mathbf{p}^{\mathbf{k}} = \lambda_i \sum_{\mathbf{k}} H_{i,\mathbf{k}}\mathbf{p}^{\mathbf{k}} + g_{1i}(\mathbf{h}), \tag{21}$$

where $\mathbf{e}_j$ denotes a unit vector; it has a one in its jth element and zeros elsewhere. The arrays $H_{i,\mathbf{k}}$ and $R_{j,\mathbf{k}}$ are obtained by matching the polynomial orders $|\mathbf{k}| = 1, 2, \cdots, P$ in Eq. (21). It is worth mentioning that the system has more variables to solve for than equations available. In order to address this, the terms in $R_{j,\mathbf{k}}$ must be *assumed*, and the approach chosen to do so determines the *style of parameterization* (Haro *et al.*, 2016). In this work, the normal form style is used, where only the terms that cause resonance between the eigenvalues are placed in the reduced dynamics $\mathbf{r}$. In the present case, due to the Hopf bifurcation at the instability speed $\Omega = \omega_w$, the following conditions hold (Wiggins, 2003):

$$\lambda_{1,2} - (k_1\lambda_{1,2} + k_2\lambda_{1,2}^*) = 0, \tag{22}$$

when k_1 and k_2 are odd. The removal of these terms from Eq. (21), which consist of the odd polynomial terms, $|\mathbf{k}'| = 3, 5, 7, \cdots$, will transform the reduced dynamics into the well known Hopf normal form, which is given as (Boyaci *et al.*, 2009; Kano *et al.*, 2019),

$$\dot{p}_1 = r_1(p_1, p_2) = \lambda_1 p_1 + R_{1,(2,1)}p_1^2p_2 + R_{1,(3,2)}p_1^3p_2^2 + \mathcal{O}(|\mathbf{p}|^7), \tag{23a}$$

$$\dot{p}_2 = r_2(p_1, p_2) = \lambda_2 p_2 + R_{2,(1,2)}p_2^2p_1 + R_{2,(2,3)}p_2^3p_1^2 + \mathcal{O}(|\mathbf{p}|^7). \tag{23b}$$

The above equations can be rewritten into polar coordinates by making $p_1 = ae^{\mathrm{i}\theta}$ and $p_2 = ae^{-\mathrm{i}\theta}$, with $\mathrm{i} = \sqrt{-1}$, in Eq. (23a) and separating the real and imaginary parts, leading to,

$$\dot{a} = b_1 a + c_1 a^3 + d_1 a^5 + \mathcal{O}(a^7), \tag{24a}$$

$$\dot{\theta} = b_2 + c_2 a^2 + d_2 a^4 + \mathcal{O}(a^6), \tag{24b}$$

where $b_1 = \mathrm{Re}[\lambda_1]$, $b_2 = \mathrm{Im}[\lambda_1]$, $c_1 = \mathrm{Re}[R_{1,(2,1)}]$, $c_2 = \mathrm{Im}[R_{1,(2,1)}]$, $d_1 = \mathrm{Re}[R_{1,(3,2)}]$ and $d_2 = \mathrm{Im}[R_{1,(3,2)}]$. Steady-state solutions can be found by making $\dot{a} = 0$ and solving for the amplitude a in Eq. (24a). The whirl frequency can be found by substituting the steady-state amplitude in Eq. (24b) to compute $\dot{\theta}$. After the obtention of steady-state solutions using Eq. (24) or (23), one uses $\mathbf{h}(\mathbf{p})$ to obtain the response in the generalized coordinates $\mathbf{q}$, Eq. (17a). Lastly, the physical displacements are then obtained from Eq. (13).

When the speed reaches the instability point, or $\Omega = \omega_w$, a limit cycle emerges. Its stability can be evaluated based on the sign of the coefficient c_1 (Wiggins, 2003). When $c_1 < 0$, one has a *super-critical* bifurcation, which corresponds to the oil-whirl phenomenon. On the other hand, when $c_1 > 0$ one has a *sub-critical* bifurcation, which indicates an oil-whip phenomenon. The former case is considered safer, as there exists a stable operating regime after the instability (Chasalevris, 2020).

Since c_1 is essentially a cubic coefficient, one may control its value by adding a purely cubic force. This is exactly the idea behind the control force introduced in Eq. (10). Therefore, by changing the control force, one may change the type of bifurcation that occurs in the system.

Table 1: Parameters used in the simulations.

Parameter	Value
Shaft length (L)	600 mm
Shaft diameter (d)	12 mm
Disk diameter (D)	120 mm
Disk thickness (h_d)	20 mm
Young's modulus (E)	210 GPa
Poisson's ratio (ν)	0.3
Density of the material (ρ)	7800 kg·m^3
Journal diameter (d_b)	31 mm
Fluid viscosity (μ)	0.028 Pa·s
Radial clearance (c_r)	90 μm
Rotor mass (M_r)	2.45 kg
Foundation mass (M_f)	$0.1M_r$
Foundation support stiffness (K_f)	10^5 N/m
Foundation support damping (C_f)	$0.1\sqrt{K_f M_f}$

3. RESULTS AND DISCUSSION

The parameters used in the simulations are listed in Tab. 1. In order to evaluate the results given by the CMR, its results will be compared with the ones generated by MATCONT (Dhooge *et al.*, 2003), which is an open-source numerical package for MATLAB^{TM}. MATCONT utilizes a modified pseudo-arclength continuation and can be used to continue equilibria and limit cycles and detect a wide range of bifurcations.

Figure 3 shows the Hopf bifurcations that emerge for the studied system using different bearing lengths (L_b). In this figure, $\Delta\Omega = \Omega - \omega_w$, where ω_w is the instability speed, and ϵ is the dimensionless eccentricity. The figure shows that, as the instability speed is approached ($\Delta\Omega < 0$), the rotor has a stable solution, which is the equilibrium. When $\Delta\Omega = 0$, one has the emergence of limit cycles. It is worth noting that the amplitude and stability of these cycles change depending on the bearing length considered. When $L_b = 17.5$ mm, one has stable cycles emerging from the bifurcation, while when $L_b = 20$ mm, the cycles are unstable. These two cases would correspond to purely oil-whirl and oil-whip, respectively. On the other hand, when $L_b = 18.75$ mm, one has the emergence of a stable cycle, which is later turned into an unstable one. This is the result of a second bifurcation, known as a fold or saddle-node bifurcation (Chouchane and Amamou, 2011). Therefore, one would experience this case as the rotor first enters oil-whirl and then oil-whip. Lastly, one notes great agreement between the CMR and MATCONT results, showing that the former can be used accurately to study the bifurcations.

Figures 4 and 5 show the transient response of the rotor before and after the instability speed, measured at the bearings, when initial conditions are close to the limit cycles. For $L_b = 20$ mm, there exists an unstable limit cycle prior to the bifurcation point. As Fig. 4a shows, an initial condition outside this cycle will lead to rising amplitudes, in this case, oil-whip. On the other hand, an initial condition inside the cycle is a stable solution, and the rotor tends to its equilibrium position. When the bifurcation point is exceeded, Figure 4b shows that there is only one unstable solution. Hence, any initial condition will lead to oil-whip. A different behavior is seen when $L_b = 17.5$ mm, as shown in Fig. 5. Firstly, there is no unstable cycle prior to the bifurcation (Fig. 5a). Secondly, after the instability speed is reached, there emerges a stable cycle. Any initial condition here will tend towards this cycle, as shown in Fig. 5b. This stable cycle is the oil-whirl phenomenon, and it can be considered safe provided the amplitude of the limit cycle is small.

From the results of Figs. 4 and 5, one can conclude that the case where $L_b = 17.5$ mm is safer than the others since the rotor can operate at least 5 rpm from the instability speed. In case $L_b = 18.75$ mm or $L_b = 20$ mm, the rotor not only

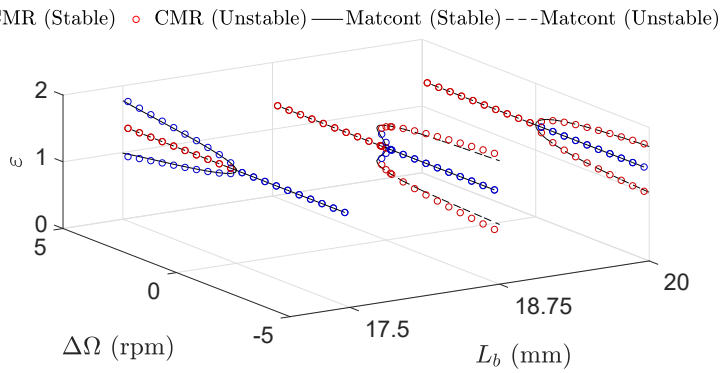

Figure 3: Effect of bearing length on Hopf bifurcation. The displacements are measured at bearing 1.

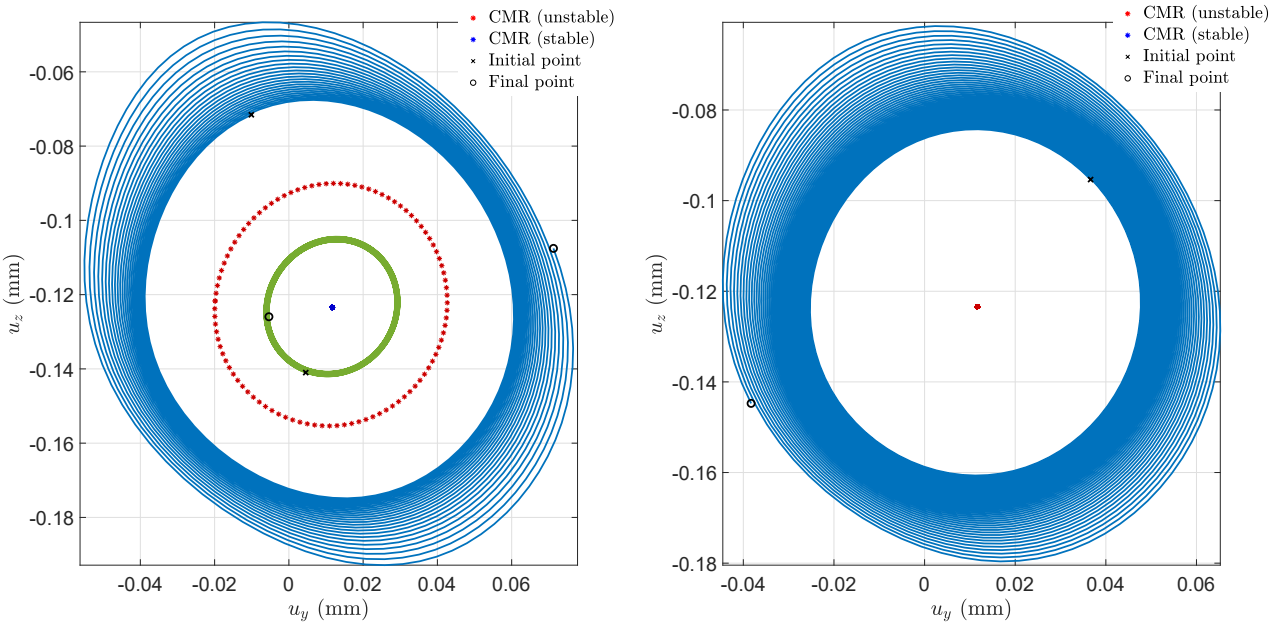

(a) (b)

Figure 4: Transient simulations for $L_b = 20$ mm and: $\Delta\Omega = -5$ rpm (a) and $\Delta\Omega = 5$ rpm (b).

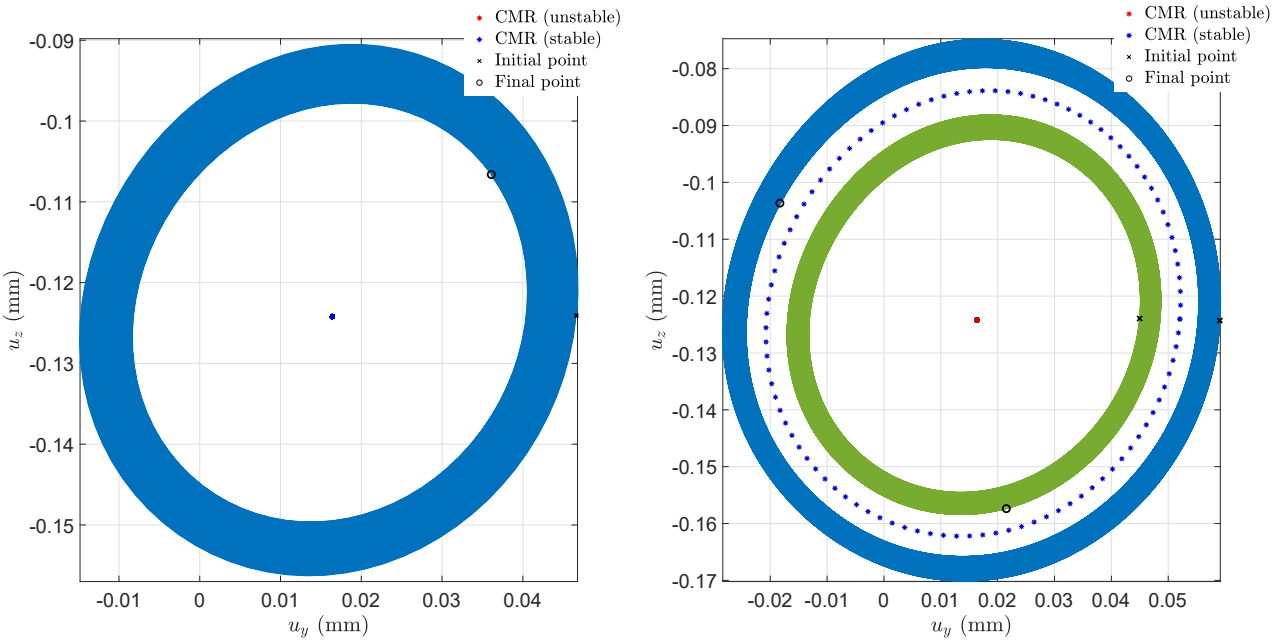

(a) (b)

Figure 5: Transient simulations for $L_b = 17.5$ mm and: $\Delta\Omega = -5$ rpm (a) and $\Delta\Omega = 5$ rpm (b).

does not have a stable solution after the bifurcation, but it can enter oil-whip before reaching the instability speed, if, for example, a strong enough perturbation is given to it. However, there may be other design requirements that inhibit the use of the value $L_b = 17.5$ mm for the bearing length, and the final rotor may present a behavior similar to the other more dangerous cases. In such situations, the idea of the control force may be useful.

The control force can be used to perform two things: to change the type of bifurcation, and to reduce the amplitude of the limit cycles. Figure 6 shows the effect of this force, which acts in the foundation, to change the limit cycles that emerge in the Hopf bifurcation. As shown in Eq. (10), the control force only takes one parameter, namely γ. In Fig. 6a, the force is used to significantly reduce the amplitude of the stable limit cycles, while in Fig. 6b, one is able to change the

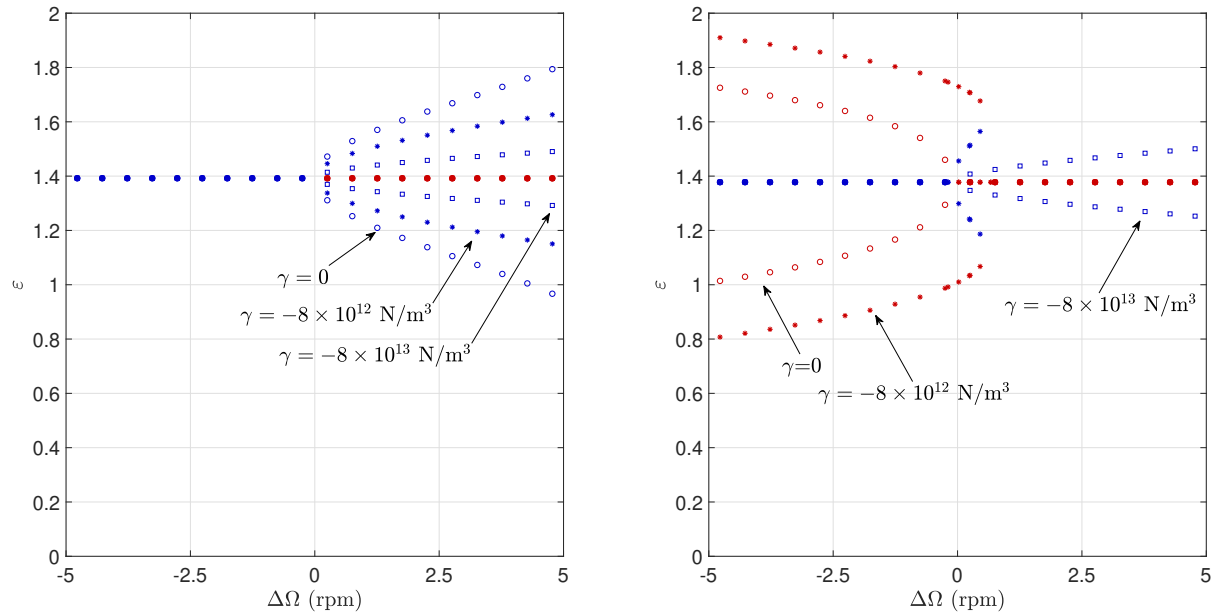

(a) (b)

Figure 6: Controlling Hopf bifurcations: reducing the stable limit cycles amplitudes ($L_b = 17.5$ mm) (a) and changing the type of bifurcation ($L_b = 20$ mm) (b).

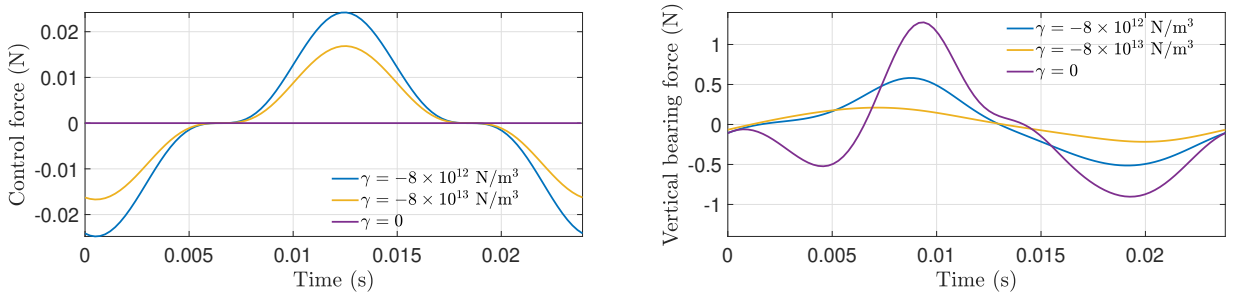

(a) (b)

Figure 7: Effect of the control on the forces for the case with $L_b = 17.5$ mm and $\Delta\Omega = 5$ rpm during one cycle: control force (a) and vertical bearing force (b).

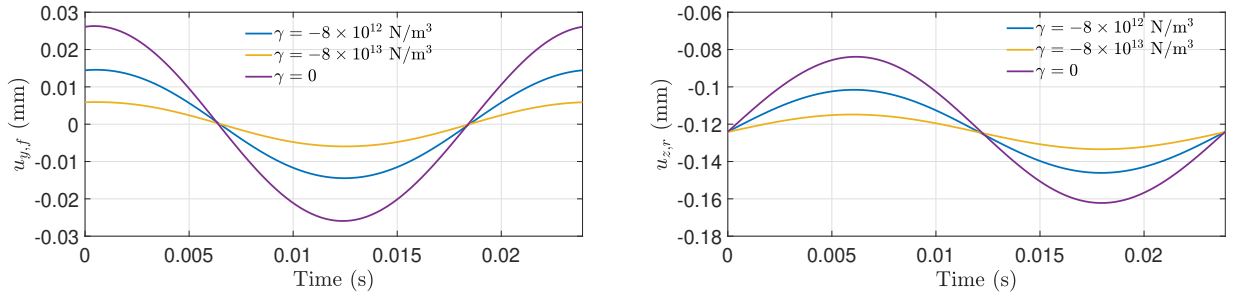

(a) (b)

Figure 8: Effect of the control on the displacements for the case with $L_b = 17.5$ mm and $\Delta\Omega = 5$ rpm during one cycle: horizontal displacement of foundation (a) and vertical displacement of rotor at the bearing (b).

type of bifurcation altogether. Since the control force acts in the horizontal direction, it does not change the equilibrium position, as the results show, and solely acts to affect the limit cycles. The force also does not change the instability speed – hence it does not affect other design requirements.

Figure 7 shows the effect of the control on the forces of the system. The behavior of the control force is what one would expect of a purely cubic nonlinearity, as Fig. 7a shows. It is interesting to note that the bearing forces are reduced when the control coefficient is changed from $\gamma = -8 \times 10^{-12}$ N/m^3 to $\gamma = -8 \times 10^{-13}$ N/m^3, as shown in Fig. 7b. This occurs due to the reduction of the amplitude of the limit cycle, as Fig. 8 shows. Therefore, the control also diminishes the transmitted forces to the foundation, which also means reduced noise. In addition, it is worth mentioning the small control forces required to alter the limit cycles. The peak control force in Fig. 7a reaches about 0.024 N, which corresponds to around 0.1 % of the rotor weight. This fact allows the use of a relatively small actuator in the eventual implementation of the approach in a real machine.

4. CONCLUSIONS

This work presented the application of the Center Manifold Reduction (CMR) method to study rotor-foundations systems subjected to Hopf bifurcations. The method was evaluated by comparing its results with the numerical package MATCONT. The results show that the CMR can be used to accurately predict the limit cycles that arise after the bifurcations. The stability of the limit cycles was shown to depend on the bearing parameters, where stable cycles correspond to the phenomenon of oil-whirl, and unstable to oil-whip. The former is generally favorable, as it allows the system to operate safely near and closely past the instability speed.

In addition, a proposed control force in the foundation allows one to modify the limit cycles that emerge in the bifurcation. With this approach, one can reduce the size of the cycles and change the type of bifurcation altogether. This procedure can be useful in situations where some design requirements lead to an oil-whip phenomenon in the rotating machine. Then the control force can be applied in the machine's foundation to change the oil-whip to oil-whirl, without affecting other design parameters.

The next step in this research would be to consider the effect of the actuator force on the global bifurcations of the rotor and to consider different bearing geometries such as lemon bore and tilting pad.

5. ACKNOWLEDGEMENTS

The authors would like to thank CNPq (Grants #307941/2019-1 and #140275/2021-5) for the financial support to this research.

6. REFERENCES

Boyaci, A., Hetzler, H., Seemann, W., Proppe, C. and Wauer, J., 2009. "Analytical bifurcation analysis of a rotor supported by floating ring bearings". *Nonlinear Dynamics*, Vol. 57, No. 4, pp. 497–507. ISSN 1573-269X. doi:10.1007/s11071-008-9403-x.

Cavalca, K.L. and Okabe, E.P., 2011. "On the Analysis of Rotor-Bearing-Foundation Systems". In K. Gupta, ed., *IUTAM Symposium on Emerging Trends in Rotor Dynamics*. Springer Netherlands, Dordrecht, pp. 89–101. ISBN 978-94-007-0020-8. doi:10.1007/978-94-007-0020-8$_8$.

Chasalevris, A., 2020. "Stability and Hopf bifurcations in rotor-bearing-foundation systems of turbines and generators". *Tribology International*, Vol. 145, p. 106154. ISSN 0301-679X. doi:10.1016/j.triboint.2019.106154.

Chouchane, M. and Amamou, A., 2011. "Bifurcation of limit cycles in fluid film bearings". *International Journal of Non-Linear Mechanics*, Vol. 46, No. 9, pp. 1258–1264. ISSN 0020-7462. doi:10.1016/j.ijnonlinmec.2011.06.005.

Dhooge, A., Govaerts, W., Kuznetsov, Yu.A., Mestrom, W. and Riet, A.M., 2003. "Cl_matcont: A continuation toolbox in Matlab". In *Proceedings of the 2003 ACM Symposium on Applied Computing - SAC '03*. ACM Press, Melbourne, Florida, p. 161. ISBN 978-1-58113-624-1. doi:10.1145/952532.952567.

Friswell, M.I., Penny, J.E.T., Seamus, D.G. and Lees, A.W., 2010. *Dynamics of Rotating Machines*. Cambridge University Press, New York.

Haro, À., Canadell, M., Figueras, J.L., Luque, A. and Mondelo, J.M., 2016. *The Parameterization Method for Invariant Manifolds: From Rigorous Results to Effective Computations*, Vol. 195 of *Applied Mathematical Sciences*. Springer International Publishing, Cham. ISBN 978-3-319-29660-9 978-3-319-29662-3. doi:10.1007/978-3-319-29662-3.

Kano, H., Ito, M. and Inoue, T., 2019. "Order reduction and bifurcation analysis of a flexible rotor system supported by a full circular journal bearing". *Nonlinear Dynamics*, Vol. 95, No. 4, pp. 3275–3294. ISSN 1573-269X. doi:10.1007/s11071-018-04755-z.

Lee, C.W., 1993. *Vibration Analysis of Rotors*. Springer Science & Business Media, Dordrecht, Netherlands, 1st edition.

Mereles, A., Alves, D.S. and Cavalca, K.L., 2023. "Model reduction of rotor-foundation systems using the approximate invariant manifold method". *Nonlinear Dynamics*. ISSN 1573-269X. doi:10.1007/s11071-023-08421-x.

Miraskari, M., Hemmati, F. and Gadala, M.S., 2017. "Nonlinear Dynamics of Flexible Rotors Supported on Journal Bearings—Part I: Analytical Bearing Model". *Journal of Tribology*, Vol. 140, No. 2. ISSN 0742-4787. doi:10.1115/1.4037730.

Muszynska, A., 1988. "Stability of whirl and whip in rotor/bearing systems". *Journal of Sound and Vibration*, Vol. 127,

No. 1, pp. 49–64. ISSN 0022-460X. doi:10.1016/0022-460X(88)90349-5.

Ponsioen, S., Jain, S. and Haller, G., 2020. "Model reduction to spectral submanifolds and forced-response calculation in high-dimensional mechanical systems". *Journal of Sound and Vibration*, Vol. 488, p. 115640. ISSN 0022460X. doi: 10.1016/j.jsv.2020.115640.

Troger, H. and Steindl, A., 1991. *Nonlinear Stability and Bifurcation Theory*. Springer Vienna, Vienna. ISBN 978-3-211-82292-0 978-3-7091-9168-2. doi:10.1007/978-3-7091-9168-2.

Wang, J.K. and Khonsari, M.M., 2006. "Bifurcation Analysis of a Flexible Rotor Supported by Two Fluid-Film Journal Bearings". *Journal of Tribology*, Vol. 128, No. 3, pp. 594–603. ISSN 0742-4787. doi:10.1115/1.2197842.

Wiggins, S., 2003. *Introduction to Applied Nonlinear Dynamical Systems and Chaos*, Vol. 2 of *Texts in Applied Mathematics*. Springer-Verlag, New York. ISBN 978-0-387-00177-7. doi:10.1007/b97481.

7. RESPONSIBILITY NOTICE

The authors are solely responsible for the printed material included in this paper.